[Research Paper] 대한금속·재료학회지 (*Korean J. Met. Mater.*), Vol. 56, No. 4 (2018) pp.304-312
DOI: 10.3365/KJMM.2018.56.4.304

Enhanced Electrical Properties and Stability of Solution-processed Amorphous Oxide Thin Film Transistors with Multi-active Layers

Won Seok Choi, Byung Jun Jung, and Myoung Seok Kwon*

Department of Materials Science and Engineering, The University of Seoul, Seoul 02504, Republic of Korea

Abstract: We investigated the electrical properties and gate bias stress stability of solution-processed amorphous oxide thin film transistors (TFTs) with multi-stacked active layers. With the multi-layered InZnO (In:Zn = 1:1), mobility was increased from 4.6 to 21.2 $cm^2V^{-1}s^{-1}$ and the subthreshold swing (SS) was improved from 0.71 to 0.54 V/decade compared to the single-layered InZnO TFT. The tri-layered InZnO TFT showed a reduced threshold voltage shift (ΔV_{th}) under positive bias stress (PBS) from +4.4 to + 0.9 V, whereas ΔV_{th} under negative bias stress (NBS) deteriorated from -0.03 to -1.5 V. We also fabricated bi-layered (bottom/top layer) TFTs using different oxide compositions with InZnO (In:Zn = 7:3) and InGaZnO (In:Zn:Ga = 3:3:1) which showed high mobility and small ΔV_{th} under PBS and NBS. The InZnO/InGaZnO TFT showed a high mobility of 17 $cm^2V^{-1}s^{-1}$, SS of 0.65 V/decade, and good stability, with ΔV_{th} under PBS and NBS of +1.2 and -1.2 V, respectively. Both the electrical properties and gate bias stress (GBS) stability were better with the InZnO/InGaZnO TFT than the single-layered InZnO TFT.

(Received January 5, 2017; Accepted February 5, 2018)

Keywords: oxide thin film transistor, multi-active layers, solution-process

1. INTRODUCTION

Amorphous oxide semiconductor (AOS) thin film transistors (TFTs) have higher mobility (50~100 $cm^2V^{-1}s^{-1}$) than hydrogenated amorphous silicon (a-Si:H) TFTs (< 1 $cm^2V^{-1}s^{-1}$). It is therefore suitable for large area displays compared to low-temperature polycrystalline silicon (LTPS) TFTs, which are limited by low uniformity and high cost. Since AOS TFTs can be used for transparent and flexible displays, they are considered promising candidates for replacing conventional Si-based TFTs [1,2].

Solution-processing is a simple and low-cost method of film deposition and is advantageous for controlling the chemical composition of AOS films. Various film compositions can be made using the solution-process method [3]. For these reasons, many solution-processes such as spin coating, ink-jet printing, and spray-coating are used for AOS TFTs and have attracted much interest.

While high mobility is required to make high resolution and large area displays, the shift in threshold voltage (Vth) under gate bias stress (GBS) is fatal to current-driven devices such as an active matrix organic light-emitting diode (AM-OLED) [4]. Both good electrical properties and GBS stability are needed for TFTs. To overcome these problems, multi-layered oxide TFTs have attracted increasing attention. Kim et al. reported the improved mobility of 2.17 $cm^2V^{-1}s^{-1}$ and good stability under positive bias stress (PBS) for InGaZnO TFTs using multistacked active layers rather than a single layer [5]. Walkers et al. reported a high mobility of 19.7 $cm^2V^{-1}s^{-1}$ for a multilayer InZnO TFT from a very low concentration of the precursor solution and more than 20 coatings [6]. In addition, it required the synthesis of In and Zn precursors instead of using commercially available In and Zn compounds [6].

In these previous studies, it was reported that the enhanced mobility in solution-processed multi-layer TFTs is related to AOS film density [5,6]. Voids can be created in the process of annealing the film. These

*Corresponding Author: Myoung Seok Kwon
[Tel: +82-2-6490-2411, E-mail: mskwon@uos.ac.kr]

voids act as defects and disturb the carrier drift motion. They can be filled by additional spin-coating for the active layer. The final AOS film density was increased by multiple spin-coating and annealing [5,6].

Solution processed bi-layer metal oxide TFTs with multistacked active layers have also been reported. InGaZnO/ZnSnO [7] and InSnZnO/InGaZnO [8] TFTs showed improved performance and good stability under PBS. However, their electrical stability under negative bias stress (NBS) was not investigated. In the InSnZnO/InGaZnO TFTs, a very thin confined bottom layer is essential to achieve high mobility and low off current, due to the conductor-like InSnZnO [8]. Al or Ga doped InZnO/InZnO TFTs [9] have also exhibited enhanced performance or GBS stability. These results reported high mobility with improved stability only for PBS, or good GBS stability with reduced electrical performance. To fabricate a multi-layered TFT with good stability under GBS conditions, it is necessary to determine the origin of the Vth shift under GBS.

According to the previous studies, charge trapping or the creation of additional defect states at the interface between the dielectric and active layers affects GBS stability [10-13]. In addition, the absorption/desorption of O_2 or H_2O at the film surface is also known to be one of the origins of the Vth shift [14-17]. The aforementioned mechanisms differ, but commonly occur at the interfaces. We can thus assume that the oxide composition of the layer that adjoins interfaces such as the back-channel or dielectric/semiconductor is important for the GBS stability of multi-layered AOS TFTs. In addition, our previous report showed that the mobilities of Zr doped InZnO TFTs were decreased and the turn-on voltages (Von) were moved positively as the carrier concentration of the AOS films was decreased by doping with a carrier suppressor [18]. Also, TFTs with a high carrier density showed instability under NBS, but good stability under PBS [18]. In the case of bilayered TFTs, we considered that the bottom layer with a high carrier density mainly affects the stability of the electrical properties of the TFTs and PBS because the field-effect channel region is mainly formed in the bottom layer adjacent to the dielectric layer. We also assumed that the top layer with low concentration of oxygen vacancies was advantageous to the instability of Vth, which is related to the absorption of water under the NBS condition.

In this paper, we studied the electrical performance of solution-processed InZnO TFTs with different numbers of InZnO layers. Currently, a sputtering processed In–Ga–Zn–O (IGZO) TFT is mainstream, with a LTPS TFT in the display backplane. Therefore, we also fabricated solution-processed bi-layer AOS TFTs using InZnO (In:Zn = 7:3) and InGaZnO (In:Zn:Ga = 3:3:1), and investigated the relationship between mobility and electrical stability for PBS and NBS, to find the proper stacking sequence to overcome their trade-off relationship.

2. EXPERIMENTAL DETAILS

0.05 M indium solution, zinc solution, and gallium solution were prepared by dissolving zinc acetate dihydrate, ($Zn(CH_3COO)_2{\cdot}2H_2O$, Aldrich), indium nitrate hydrate ($In(NO_3)_2{\cdot}xH_2O$, Aldrich), and gallium nitrate hydrate ($Ga(NO_3)_3{\cdot}xH_2O$, Aldrich) in 2-methoxyethanol, with aqueous ammonia as a catalyst and acetyl acetone as a stabilizer and fuel [3]. These solutions were stirred for 1 hour at 60 °C. InZnO solution and InGaZnO solution were prepared by blending the indium, zinc, and gallium solutions. The molar ratio of In:Zn was 1:1 or 7:3 in the InZnO solution and that of In:Zn:Ga was 3:3:1 in the InGaZnO solution. The mixed solutions were stirred for 2 hours at 25 °C and filtered through a 0.20 μm PTFE syringe filter. Substrates were cleaned with acetone, deionized water, and isopropyl alcohol by sonication, and treated with UV/O_3 for 10 min using a UV-ozone cleaner (AH1700, 28 mW cm^{-2}, AHTECH LTS Co., Ltd., Korea). The InZnO and InGaZnO solutions were spin-coated at 1500 rpm for 30 sec on a heavily As-doped n-type Si wafer (resistivity < 0.005 Ω·cm) substrate with a thermally grown 1000 Å thick SiO_2 layer. The deposited film was annealed on a hot plate for 2 hours at 400 °C in ambient air. For the multi-layered TFTs, each of

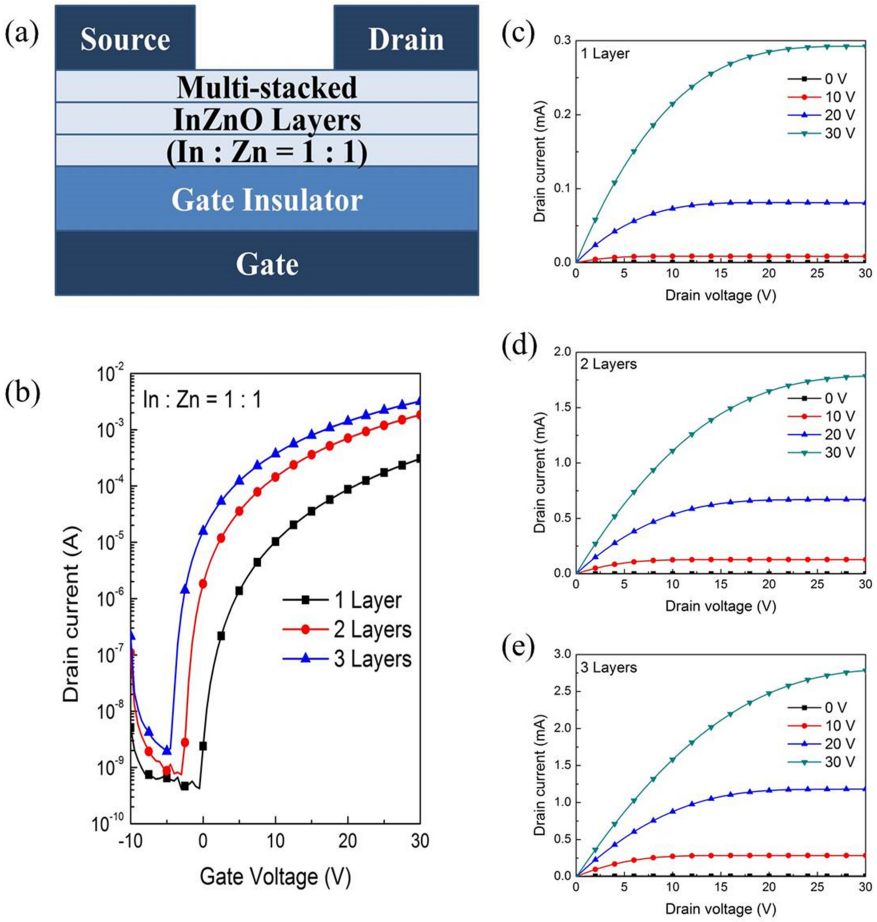

Fig. 1. (a) Structure of TFT with multi-layered InZnO layers. (b) Transfer curve with different numbers of InZnO layers. (c)-(e) Output curves with different numbers of InZnO layers.

the coated layers was annealed for 30 min at 400 °C, and then the multi-layered film was finally annealed for 2 hours at 400 °C. Aluminum source and drain electrodes with a thickness of 70 nm were deposited by thermal evaporation. The channel width (W) and length (L) were 2000 μm and 200 μm, respectively (W/L=10). The TFTs were passivated by poly (methyl methacrylate) (PMMA) to reduce the effects of ambient air. The current-voltage characteristics of the multi-layered TFTs were measured using an Agilent B2912 in air atmosphere. The electrical properties of the TFTs were extracted in the saturation regime of the TFTs. In the saturation regime, the saturated drain current is given by:

$$I_D = \frac{W}{2L} C_i \mu_{sat} (V_G - V_{th})^2 \quad (1)$$

W is the channel width and L is the channel length, μ_{sat} is the field effect mobility of the AOS film, C_i is the capacitance of the gate insulator, V_G is the gate voltage, V_{th} is the threshold voltage. The turn-on voltage (V_{on}) is the gate voltage needed to extract the subthreshold swing (SS), which is the steepness of the transfer curve for the switching characteristics of the TFT, and is given by:

$$SS = \frac{d\,V_G}{d(log_{10} I_D)} \quad (2)$$

3. RESULTS AND DISCUSSION

We first analyzed the current-voltage characteristics of the multi-layered InZnO TFTs. Fig. 1(a) shows the structure of the multi-layered InZnO (In:Zn = 1:1) TFTs

and Fig. 1(b) shows the transfer curve with single-, bi-, and tri-layered InZnO TFTs. For multi-layered InZnO TFTs, the molar ratio of In:Zn was 1:1 instead of 7:3. Since the bi-layered InZnO (In:Zn = 7:3) TFT is excessively negatively shifted, it is difficult to analyze the transfer characteristics of multi-layered InZnO TFT. The electrical properties of the bi-layered (In:Zn = 7:3) TFT will be shown later. The output characteristics of the TFTs with various InZnO layers are shown in Fig. 1(c)-1(e), which indicates that the drain current increased by adding InZnO films. In Fig. 2(b), it can also be seen that the drain current of tri-layered InZnO TFT was more than ten times that of the single-layered InZnO TFT at a gate voltage of 30 V. In addition, the transfer curve moved negatively with the increasing number of InZnO layers. This negative shift is related to the high carrier concentration of the AOS [5,8,19]. The tri-layered InZnO TFT showed a high mobility of 21.2 $cm^2V^{-1}s^{-1}$, V_{on} of -4.5 V, ON/OFF ratio of 1.6×10^6, and SS of 0.54 V/decade compared to the single-layered InZnO TFT with 4.6 $cm^2V^{-1}s^{-1}$, -0.5 V, 7.4×10^5, and 0.71 V/decade. Notably, this shows that the saturation mobility of the tri-layered TFT was more than four times that of the single-layered TFT. It is known that this improvement in mobility can be attributed to fill the pin-holes close to the dielectric layer and the dense AOS film, due to the over coating process [5,6]. In our results, only three times coating of the combustion sol-gel InZnO solution provided the high mobility, which was comparable to that in the previous report using a very low concentration of the precursor solution [6].

Figure 2 shows the GBS stability of the multi-layered InZnO TFTs. The changes in transfer curve with different numbers of InZnO layers under PBS and NBS are shown in Fig. 2(a)-2(c). A GBS test was performed with ±20 V gate voltage and 10 V drain voltage for 1000 sec. Figure 2 indicates that the PBS stability was improved, whereas the NBS stability deteriorated as the number of InZnO layers was increased. The single-layered InZnO TFT showed ΔV_{th} under PBS of +4.4 V and ΔV_{th} under NBS of -0.03 V compared with the tri-layered InZnO TFT with +0.9 V and -1.5 V, respectively. The electrical properties and ΔV_{th} under GBS of the multi-layered InZnO TFTs are shown as Table 1.

Figure 3(a) shows the bi-layered structure of TFTs using InZnO (In:Zn = 7:3) and InGaZnO (In:Zn:Ga = 3:3:1). Ga is an oxygen getter and acts as the carrier suppressor in amorphous InGaZnO thin films [3]. Therefore, an InGaZnO layer was introduced in this bi-layer TFTs for the stability of the NBS. The composition of the bi-layered TFT was marked as the bottom/top layer, and the transfer curve of the bi-layered TFT is shown in Fig. 3(b). Like the multi-layered InZnO TFTs, the InZnO/InZnO and InGaZnO/InGaZnO TFTs showed increased mobility and a negative shift in Vth in comparison with the single-layered InZnO and InGaZnO TFTs. In the case of bi-layered TFTs using InZnO and InGaZnO, the TFTs exhibited different performance according to the stacking sequence. The InZnO/InGaZnO TFT exhibited a mobility of 17 $cm^2V^{-1}s^{-1}$, V_{on} of -5.5 V, ON/OFF ratio of 2.1×10^6, and SS of 0.65 V/decade compared to the InGaZnO/InZnO TFT with 13.8 $cm^2V^{-1}s^{-1}$, -3.0 V, 2.6×10^6, 0.63 V/decade. Considering that the mobility of the InZnO TFT was higher than that of the InGaZnO TFT shown in Table 2, the transfer characteristics of the bi-layered TFTs were affected by the oxide composition of the bottom layer. This result also agrees with the results from the previous studies [9,20]. Figure 4(a)-4(c) show the GBS stability of the InZnO, InZnO/InGaZnO, and InGaZnO/InZnO TFTs. The GBS stability differed according to the oxide composition of the bottom and top layer. The InZnO/InGaZnO TFT showed ΔV_{th} under a PBS of +1.2 V and ΔV_{th} under a NBS of -1.2 V compared to the InZnO TFT with +1.9 V and -1.3 V, respectively. This result shows that the InZnO/InGaZnO TFT was more stable than the InZnO TFT under both PBS and NBS conditions. On the other hand, the InGaZnO/InZnO TFT was more unstable than the InZnO TFT under both GBS conditions, with ΔVth under PBS of +3.6 V and ΔV_{th} under NBS of -2.1 V.

In previous reports, the Vth shift was shown to

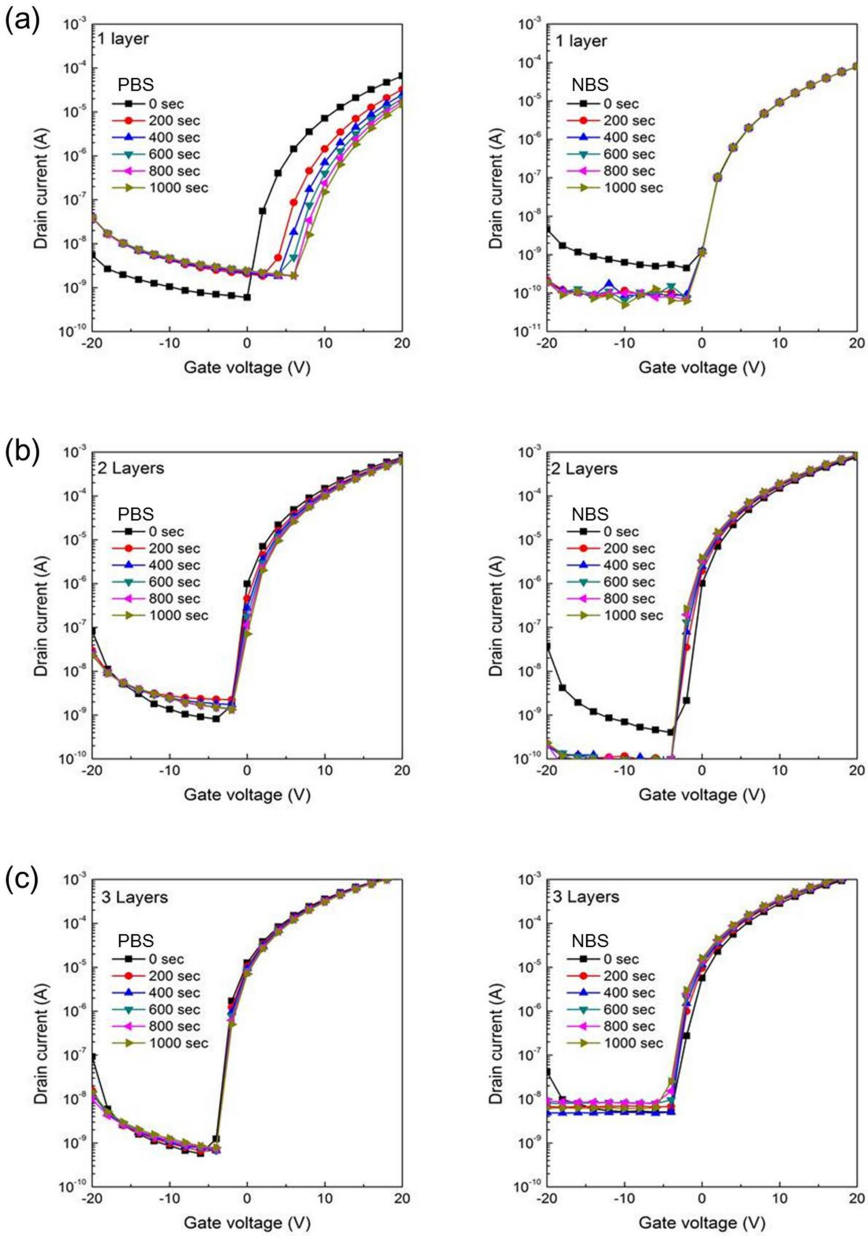

Fig. 2. Positive and negative bias stress stability of (a) single-layered InZnO, (b) bi-layered InZnO, and (c) tri-layered InZnO TFTs.

Table 1. Electrical properties of the TFTs with different numbers of InZnO layers.

Number of layers	μ_{sat} ($cm^2V^{-1}s^{-1}$)	V_{on} (V)	ON/OFF ratio	S.S (V/decade)	PBS ΔV_{th} (V)	NBS ΔV_{th} (V)
1	4.6	-0.5	7.4×10^5	0.71	4.4	-0.03
2	15.7	-3.0	2.5×10^6	0.60	1.4	-1.1
3	21.2	-4.5	1.6×10^6	0.54	0.9	-1.5

occur due to three different mechanisms. In the first mechanism, electrons are injected into the dielectric and then become trapped [10]. The second mechanism involves the creation of additional defect states at the dielectric/semiconductor interface [11]. The third mechanism is the absorption/desorption of ambient gas

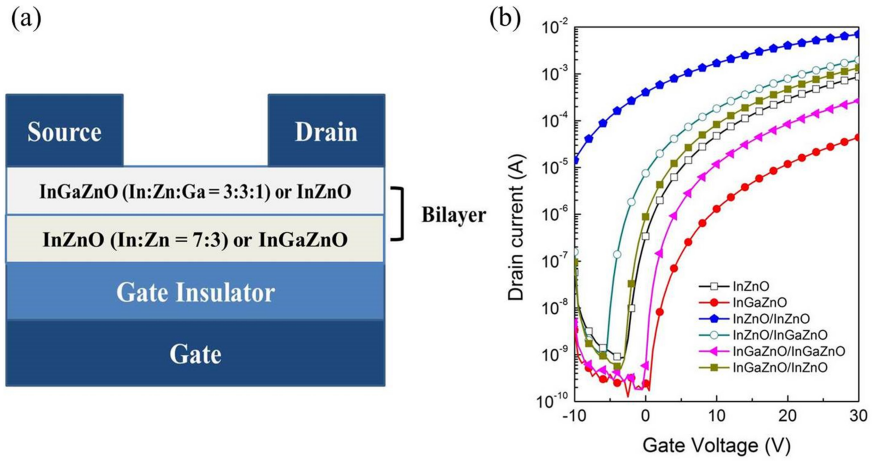

Fig. 3. (a) Structure of bi-layered TFTs using InZnO and InGaZnO films. (b) Transfer characteristics of single-layered InZnO (In:Zn = 7:3), InGaZnO (In:Zn:Ga = 3:3:1), bi-layered InZnO/InZnO, InGaZnO/InGaZnO, InZnO/InGaZnO, and InGaZnO/InZnO TFTs.

such as O_2 or H_2O at the film surface [14-17]. Charge trapping in the dielectric is a dominant mechanism for the Vth shift of TFTs using SiN_x as a dielectric. In the case of SiO_2, it is known that the additional defect state results in the instability of the Vth [10,11,21]. With the creation of the additional defects, when a positive gate voltage is applied, acceptor states are formed and cause electron trapping at the dielectric/semiconductor interface [22,23]. In contrast, the donor states result in hole trapping at the interface due to negative gate bias stress. V_O is expecially known to be a deep donor [12] and can be ionized into V_O^+ or V_O^{2+} related to hole trapping [13]. The instability of the Vth is also affected by the absorption/desorption of O_2 or H_2O at the back-channel. When oxygen molecules are absorbed at the film surface, oxygen can capture electrons from the film. This depletes the electrons and Vth is shifted positively. Under the NBS condition, the absorbed H_2O can donate electrons to the film. Therefore, the electron concentration in the film will increase and a negative Vth shift occurs [14-17].

Street *et al.* reported that solution-processed TFTs with high mobility were stable under PBS [24]. The results in Table 2 indicate that the InZnO TFT exhibited high mobility and good stability under PBS compared to the InGaZnO TFT, which is consistent with the previous results [24]. In addition, the TFTs with low mobility have more acceptor states in the deep levels [25]. Therefore, it can be expected that InGaZnO films have deeper acceptors than the InZnO films. In our previous result, the stability of the InZnO TFTs was improved by adding a carrier suppressor [18]. Likewise, the PBS stability of the InGaZnO TFT was inferior to that of the InZnO TFT, and in the case of NBS, the stability of the InGaZnO TFT was better than that of the InZnO TFT. The GBS stability of these two oxide compositions differs and the stability of the bi-layered TFTs using InZnO and InGaZnO varies according to the oxide composition of the bottom/top layer. This means that the position of the oxide layer can affect the stability of the bi-layered TFTs.

As mentioned above, the InZnO/InGaZnO TFT was more stable than the InZnO TFT under both the PBS and NBS, but InGaZnO/InZnO TFT aggravated the instability of the Vth under PBS and NBS. This result indicates that the oxide composition of the bottom layer has an effect on the PBS stability, and that of the top layer influences the NBS stability. That is, in terms of the GBS stability of the bi-layered TFTs, it can be assumed that the Vth shift under PBS is mainly related to the dielectric/semiconductor interface and the instability of the Vth under NBS is affected by the condition of the back-channel. When a positive gate voltage is applied, the

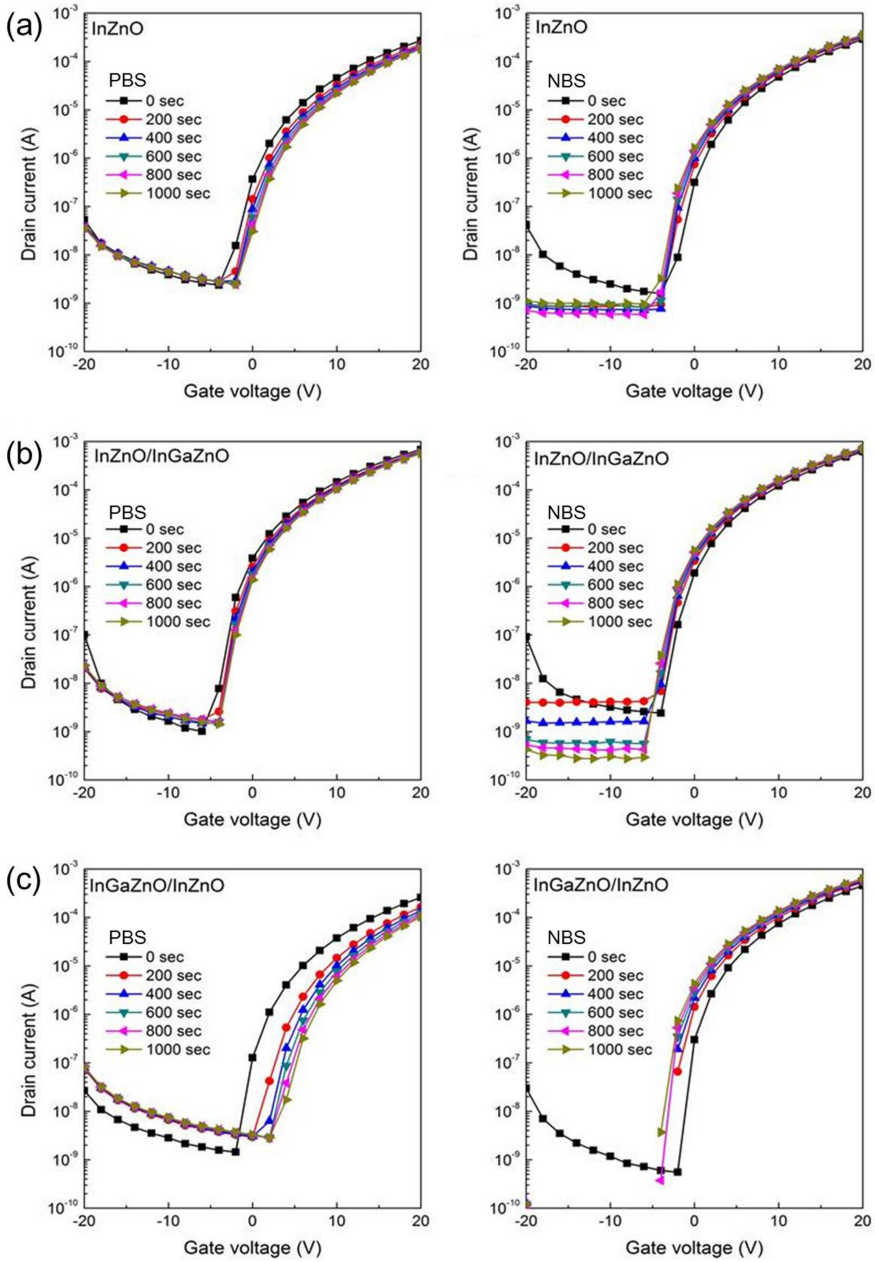

Fig. 4. Positive and negative bias stress stability of (a) InZnO, (b) InZnO/InGaZnO, and (c) InGaZnO/InZnO TFTs

Table 2. Electrical properties of the TFTs with various bilayer structures.

Bottom/Top	μ_{sat} ($cm^2V^{-1}s^{-1}$)	V_{on} (V)	ON/OFF ratio	S.S (V/decade)	PBS ΔV_{th} (V)	NBS ΔV_{th} (V)
InZnO	10	-3	1.1×10^6	0.86	1.9	-1.3
InGaZnO	0.7	0.5	3.5×10^5	0.85	6.6	-
InZnO/InZnO	Conductive					
InZnO/InGaZnO	17	-5.5	2.1×10^6	0.65	1.2	-1.2
InGaZnO/InGaZnO	3.3	0	1.5×10^6	0.64	8.5	-
InGaZnO/InZnO	13.8	-3	2.6×10^6	0.63	3.6	-2.1

Fermi level in the AOS is close to the conduction band. Therefore, the formation enthalpy of the acceptor states is reduced and additional acceptor states such as cation vacancies (V_M^-, V_M^{2-}) are created [23]. These defect states cause electron trapping near the dielectric/semiconductor, which results in a positive Vth shift. It can be deduced that the NBS stability of the bi-layered TFT is mainly related to the absorption/desorption of O_2 or H_2O. The absorption of O_2 is known to have the following reaction [14].

$$O_2(gas) + e^- \leftrightarrow O_2^- \quad (solid) \tag{3}$$

When oxygen molecules are absorbed on a surface, the oxygen can capture electrons, reducing the carrier density of the AOS film. In contrast, absorbed H_2O can donate electrons to the film, and thus a negative Vth shift occurs. Orui *et al.* reported that –OH chemical bonding originated with H_2O and these bonding states formed deep donor states [26].

$$\text{-M-OH} + \text{-M′-OH} \leftrightarrow \text{-M-} + \text{-M′-O} + H_2O\ (gas) \tag{4}$$

Therefore, hydrogen from H_2O is ionized and forms –OH chemical bonds by donating free electrons to the AOS film [27]. Under NBS condition, the formation enthalpy of donor states decreases [23], whereas the formation energy of O_2^- is increased [28]. Therefore, -OH bonding is formed more by the absorption of H_2O, resulting in O_2 desorption. As a result, the Vth shifts negatively due to the increasing electron density of the films. Nomura *et al.* reported that near-VBM states such as V_O are concentrated on the AOS film surface. As shown in reaction (4), the V_O concentration of the film is related to the absorption of H_2O. It is known that the V_O concentration of InGaZnO films is less than that of InZnO films. Therefore, it can be deduced that InGaZnO films are effective in protecting the back-channel from ambient air.

Recently, sensor applications using oxide TFTs have attracted attention [29,30]. As a receptor and transducer the TFT is usually exposed in the ambient environment of the target. Therefore, in continuous real-time monitoring, its electrical stability in humidity or water is important, to ensure a stable baseline. Solution processable oxide TFTs can be easily fabricated with different compositions and multi-active layers, making them good candidates for various sensors, with high operating stability and high mobility. For high mobility and stability under PBS, multiple coating of a sol-gel solution and a bottom layer with a high carrier concentration are useful. In addition, a top layer with a low carrier concentration can provide the the stability under NBS.

4. CONCLUSION

Multi-layered TFTs were fabricated via the solution-process method. As the number of InZnO layers increased, the mobility increased drastically and the threshold voltage shifted negatively. In the case of GBS stability, PBS stability was improved but NBS stability deteriorated.

The bi-layered TFTs were fabricated using InZnO and InGaZnO, and the GBS stability was investigated using different stacking sequences. The InZnO/InGaZnO TFT exhibited higher saturation mobility and better stability under both PBS and NBS than the InZnO TFT. This result shows that PBS stability is mainly related to electron trapping due to the additional acceptor states at the dielectric/semiconductor interface, and the instability under NBS is affected by the absorption of H_2O and desorption of O_2 at the AOS film surface. Therefore, engineering of each layer in the multi-active layers can provide stability under both PBS and NBS when a AOS layer with a high carrier concentration is placed on the dielectric layer and a AOS layer with a low carrier concentration is located on the back-channel.

ACKNOWLEDGEMENTS

This work was supported by the 2015 Research Fund of the University of Seoul for Myoung Seok Kwon. This work was also supported by a grant from the Basic Science Research Program through the National Research Foundation of Korea (NRF), funded by the Ministry of Science, ICT, and Future Planning (NRF-2012R1A1A1043460), awarded to the Byung Jun Jung.

REFERENCES

1. T. Kamiya, K. Nomura, and H. Hosono, *Sci. Technol. Adv. Mater.* **11,** 044305 (2010).
2. E. Fortunato, P. Barquinha, and R. Martins, *Adv. Mater.* **24**, 2945 (2012).
3. J. W. Hennek, J. Smith, A. Yan, M.-G. Kim, W. Zhao, V. P. Dravid, A. Facchetti, and T. J. Marks, *J. Am. Chem. Soc.* **135**, 10729 (2013).
4. J.-H. Lee, W.-J. Nam, K.-S. Shin, and M.-K. Han, *J. Non-Cryst. Solids* **352**, 1719 (2006).
5. D. J. Kim, D. L. Kim, Y. S. Rim, C. H. Kim, W. H. Jeong, H. S. Lim, and H. J. Kim, *ACS Appl. Mater. Interfaces* **4**, 4001 (2012).
6. D. E. Walker, M. Major, M. B. Yazdi, A. Klyszcz, M. Haeming, K. Bonrad, C. Melzer, W. Donner, and H. von Seggern, *ACS Appl. Mater. Interfaces* **4**, 6835 (2012).
7. C. H. Kim, Y. S. Rim, and H. J. Kim, *ACS Appl. Mater. Interfaces* **5**, 6108 (2013).
8. Y. S. Rim, H. Chen, X. Kou, H. S. Duan, H. Zhou, M. Cai, H. J. Kim, and Y. Yang, *Adv. Mater.* **26**, 4273 (2014).
9. J.-S. Seo and B.-S. Bae, *ACS Appl. Mater. Interfaces* **6**, 15335 (2014).
10. A. A. Fomani and A. Nathan, *J. Appl. Phys*. **109**, 084521 (2011).
11. M. J. Powell, C. van Berkel, A. R. Franklin, S. C. Deane, and W. I. Milne, *Phys. Rev. B* **45**, 4160 (1992).
12. K. Nomura, T. Kamiya, E. Ikenaga, H. Yanagi, K. Kobayashi, and H. Hosono, *J. Appl. Phys.* **109**, 073726 (2011).
13. S. An, M. Mativenga, Y. Kim, and J. Jang, *Appl. Phys. Lett.* **105**, 053507 (2014).
14. J. K. Jeong, H. W. Yang, J. H. Jeong, Y.-G. Mo, and H. D. Kim, *Appl. Phys. Lett.* **93**, 123508 (2008).
15. D. Kang, H. Lim, C. Kim, I. Song, J. Park, Y. Park, and J. Chung, *Appl. Phys. Lett.* **90**, 192101 (2007).
16. J. S. Park, J. K. Jeong, H. J. Chung, Y. G. Mo, and H. D. Kim, *Appl. Phys. Lett.* **92**, 072104 (2008).
17. F. H. Chen, T. M. Pan, C. H. Chen, J. H. Liu, W. H. Lin, and P. H. Chen, *IEEE Electron Device Lett.* **34**, 635 (2013).
18. W. S. Choi, H. Jo, M. S. Kwon, and B. J. Jung, *Curr. Appl. Phys.* **14**, 1831 (2014).
19. J.-S. Park, J. K. Jeong, Y.-G. Mo, H. D. Kim, and C.-J. Kim, *Appl. Phys. Lett.* **93**, 033513 (2008).
20. J. C. Park and H. N. Lee, *IEEE Electron Device Lett.* **33**, 818 (2012).
21. J. K. Jeong, *J. Mater. Res.* **28**, 2071 (2013).
22. K. Nomura, T. Kamiya, M. Hirano, and H. Hosono, *Appl. Phys. Lett.* **95**, 013502 (2009).
23. J. G. Um, M. Mativenga, P. Migliorato, and J. Jang, *J. Appl. Phys.* **115**, 134502 (2014).
24. R. A. Street, T. N. Ng, R. A. Lujan, I. Son, M. Smith, S. Kim, T. Lee, Y. Moon, and S. Cho, *ACS Appl. Mater. Interfaces* **6**, 4428 (2014).
25. K. H. Lee, K. C. Ok, H. Kim, and J. S. Park, *Ceram. Int.* **40**, 3215 (2014).
26. T. Orui, J. Herms, Y. Hanyu, S. Ueda, K. Watanabe, I. Sakaguchi, N. Ohashi, H. Hiramatsu, H. Kumomi, H. Hosono, and T. Kamiya, *J. Disp. Technol.* **11**, 518 (2015).
27. K. Nomura, T. Kamiya, and H. Hosono, *ECS J. Solid State Sci. Technol*. **2**, P5 (2013).
28. W.-T. Chen, S.-Y. Lo, S.-C. Kao, H.-W. Zan, C.-C. Tsai, J.-H. Lin, C.-H. Fang, and C.-C. Lee, *IEEE Electron Device Lett*. **32**, 1552 (2011).
29. Y. S. Rim, H. Chen, B. Zhu, S.-H. Bae, S. Zhu, P. J. Li, I. C. Wang, and Y. Yang, *Adv. Mater. Interfaces* **4**, 1700020 (2017).
30. J. Jung, S. J. Kim, T. S. Jung, J. Na, D. H. Yoon, M. M. Sabri, and H. J. Kim, *IEEE Trans. Electron Devices* **64**, 515 (2017).